Liquid Crystals
Publication details, including instructions for authors and subscription information:
http://www.informaworld.com/smpp/title~content=t713926090

Structure of *trans*-4-(trans-4-*n*-pentylcyclohexyl)cyclohexylcarbonitrile (CCH5) in the isotropic and nematic phases: a computer simulation study

M. R. Wilson[a]; M. P. Allen[b]
[a] School of Physics and Materials, Lancaster University, Lancaster, England [b] H. H. Wills Physics Laboratory, Royal Fort, Bristol, England

To cite this Article Wilson, M. R. and Allen, M. P.(1992) 'Structure of *trans*-4-(trans-4-*n*-pentylcyclohexyl)cyclohexylcarbonitrile (CCH5) in the isotropic and nematic phases: a computer simulation study', Liquid Crystals, 12: 1, 157 — 176
To link to this Article: DOI: 10.1080/02678299208029045
URL: http://dx.doi.org/10.1080/02678299208029045

LIQUID CRYSTALS, 1992, VOL. 12, NO. 1, 157–176

Structure of *trans*-4-(*trans*-4-*n*-pentylcyclohexyl)cyclohexylcarbonitrile (CCH5) in the isotropic and nematic phases: a computer simulation study

by M. R. WILSON*
School of Physics and Materials, Lancaster University, Lancaster LA1 4YB, England

and M. P. ALLEN
H. H. Wills Physics Laboratory, Royal Fort, Tyndall Avenue, Bristol BS8 1TL, England

(*Received 30 October 1991; accepted 15 January 1992*)

We have studied the single particle structural properties of the nematogen *trans*-4-(*trans*-4-*n*-pentylcyclohexyl)cyclohexylcarbonitrile (CCH5) by molecular dynamics simulation using realistic atom–atom potentials. On going from the isotropic phase at 390 K to the nematic phase at 350 K, the molecules become significantly longer and thinner, as indicated by the equivalent molecular moment-of-inertia spheroid and the distribution of *trans* and *gauche* bonds. This change is only partly accounted for by the lowering of the temperature, there being a significant quenching effect due to the change in the molecular environment. This quenching effect is also apparent in the distribution of molecular shapes seen in molecular width-breadth contour maps. In the nematic phase, at 350 K, the distributions of alkyl tail bond orientations with respect to the director show a pronounced odd–even effect, with peaks in the distributions occurring alternately parallel to, and at an angle to, the director.

1. Introduction

The study of liquid-crystalline behaviour provides a major challenge for contemporary theorists. To some extent liquid crystals can be understood on the basis of the simplest of theories. The early work of Maier and Saupe [1] provided a convenient molecular field rationale for the existence of the nematic phase which depends on anisotropic dispersion forces. Landau–de Gennes theory on the other hand treats liquid-crystalline behaviour as a perturbation of the isotropic phase by expanding the free energy density in terms of the order parameter and its spatial derivatives [2, 3]. Prior to this Onsager had predicted that a system of hard rods could exhibit a first order transition from an isotropic liquid to an orientationally ordered phase without the need for attractive forces [4]. In this case the driving force for molecular alignment is provided by the orientational entropy. Despite the success of these theories, the need still remains for a more detailed description of liquid-crystalline phase behaviour, which at present cannot be provided by simple theory.

In recent times the substantial increase in available computer speed has led to the use of computer simulation as a tool for understanding liquid crystal phases [5]. Initial work focused on simple lattice models in which lattice spins were found to undergo a

* Author for correspondence.

0267–8292/92 $3·00

weak, first order phase transition to an orientationally ordered phase as the temperature was lowered [6]. More recently, simple, hard core model potentials have been employed, making use of both Monte Carlo and molecular dynamics techniques to sample phase space. These have been successful in demonstrating the existence of thermodynamically stable nematic and smectic phases at densities below the freezing point [7, 8]. In practice these simulations are able to provide a wealth of thermodynamic, structural and (in the case of molecular dynamics) dynamical information for mesophases, including phase diagrams, order parameters, elastic constants and transport coefficents [9]. Whilst it is essential to study the behaviour of the simplest models in some depth, in order to make progress in understanding the forces responsible for mesophase formation, the possibility also exists of extending these simple models to build in realistic features such as molecular flexibility, complicated structural anisotropy and electrostatic forces. In recent simulation work [10, 11] we have adopted a realistic atom–atom model for a mesogen in which the molecular potential is built up from a sum of site–site potentials situated on extended atoms (comprising carbons and attached hydrogens). The internal structure is modelled by a standard empirical force-field calibrated to the best available spectroscopic data. Despite the complexity of the potential and its associated expense in terms of computer time, we have produced some preliminary phase behaviour for the mesogen *trans*-4-(*trans*-4-*n*-pentylcyclohexyl)cyclohexylcarbonitrile (CCH5) (see figure 1). The full details of our simulations have been described elsewhere [11]. In brief, we have carried out molecular dynamics calculations on samples of 128 CCH5 molecules at three temperatures: 350 K and 370 K in the nematic phase (corresponding respectively to average order parameters of 0·62 and 0·38), and 390 K in the pretransitional region of the isotropic phase. The simulations were carried out for, respectively, 662, 720 and 648 ps, using the AMBER potential energy function [12]

$$V_{\text{total}} = \sum_{\text{bonds}} K_r(r - r_{\text{eq}})^2 + \sum_{\substack{\text{bending}\\ \text{angles}}} K_\theta(\theta - \theta_{\text{eq}})^2 + \sum_{\substack{\text{dihedral}\\ \text{angles}}} \frac{V_n}{2}(1 + \cos(n\phi - \gamma)) + \sum_{i<j} \left(\frac{q_i q_j}{R_{i,j}} + \frac{A_{i,j}}{R_{i,j}^{12}} - \frac{C_{i,j}}{R_{i,j}^{6}} \right), \tag{1}$$

where K_r, K_θ and V_n are force constants representing bond stretching, bond bending and torsional motion respectively. $R_{i,j}$ is the distance between atoms i and j, q_i and q_j are the partial electronic charges on atoms i and j, $A_{i,j} = (A_{i,i}A_{j,j})^{1/2}$, and $C_{i,j} = (C_{i,i}C_{j,j})^{1/2}$. $A_{i,i}$ and $C_{i,i}$ can be expressed in terms of Lennard-Jones ε and σ parameters: $A_{i,i} = 4\varepsilon_{i,i}\sigma_{i,i}^{12}$, $C_{i,i} = 4\varepsilon_{i,i}\sigma_{i,i}^{6}$. The parameters used in this potential are tabulated in [11]. We have used the SHAKE method [13] to remove the high frequency bond stretching motion and to constrain all of the bond lengths to their equilibrium values r_{eq}.

In this paper, we present some of the structural results of our model. In § 2 we describe the variation in the dihedral angle distributions which occur as a function of temperature, whilst in § 3 we represent the structural anisotropy of our model by an equivalent inertia spheroid. In § 4 bond orientational distributions are presented for various bonds in the rigid core and the alkyl chain. Finally, our conclusions are summarized in § 5. The dynamical results of our model are presented in a later paper [14].

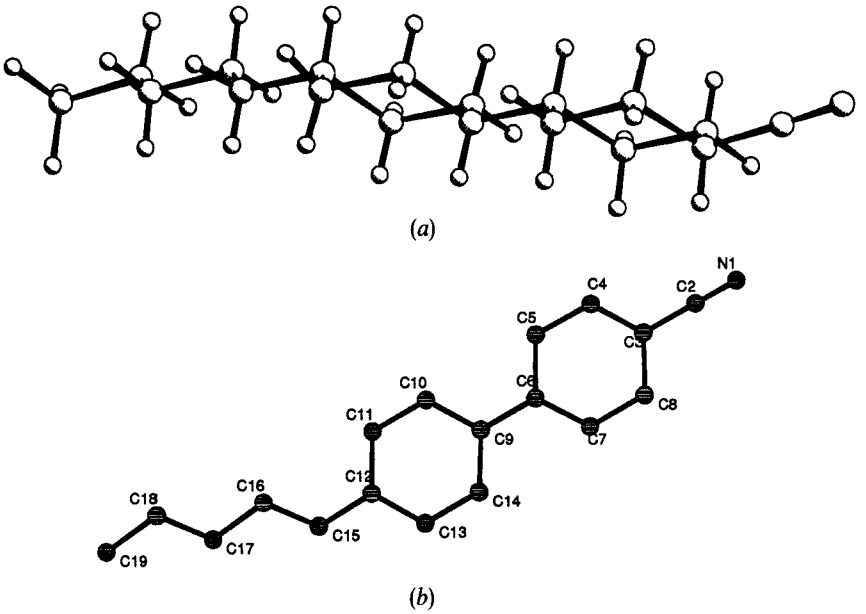

Figure 1. The CCH5 molecule in its lowest energy conformation. (*a*) Ball and stick representation, showing all atoms, with positions obtained from the crystal structure. (*b*) Simplified model, showing the labelling of united atoms.

2. Dihedral angle distributions

Dihedral angle distributions depend critically upon the shape of the effective torsional potential. In our work an explicit torsional potential with three-fold periodicity is specified for each dihedral angle by means of a third order term in the Fourier series in equation (1). For an isolated molecule, additional structure is imparted to the torsional potential by means of internal non-bonded interactions, the most significant contribution being provided by 1,4-interactions. For a molecule surrounded by neighbours in a fluid, further perturbations of the effective torsional potential can occur due to intermolecular interactions. The observed dihedral distribution $\mathscr{P}(\phi)$ can be written in terms of an effective torsional potential, or conformational free energy, $\mathscr{V}(\phi)$:

$$\mathscr{P}(\phi) = C \exp\left[-\frac{\mathscr{V}(\phi)}{k_B T} \right], \tag{2}$$

where C is a normalizing factor. The temperature dependence of $\mathscr{V}(\phi)$ reflects changes in the average environment of a molecule.

We have calculated dihedral angle distributions, and effective torsional potentials, for key torsional angles at each temperature. We monitor the three torsional angles in the alkyl chain, (defined by atoms 12–15–16–17, 15–16–17–18 and 16–17–18–19), the inter-ring torsional angle (5–6–9–14) and the torsional angle between the second cyclohexane ring and the chain (11–12–15–16). In figures 2–6 we plot the dihedral distributions and effective torsional potentials for each of these angles. We expect dihedral angle distributions to be peaked around the lowest energy conformation for each angle. For four of the dihedral angles this correponds to the *trans* conformation with $\phi = 180°$, whilst for angle 11–12–15–16, a double degeneracy occurs at $\phi = 67°$,

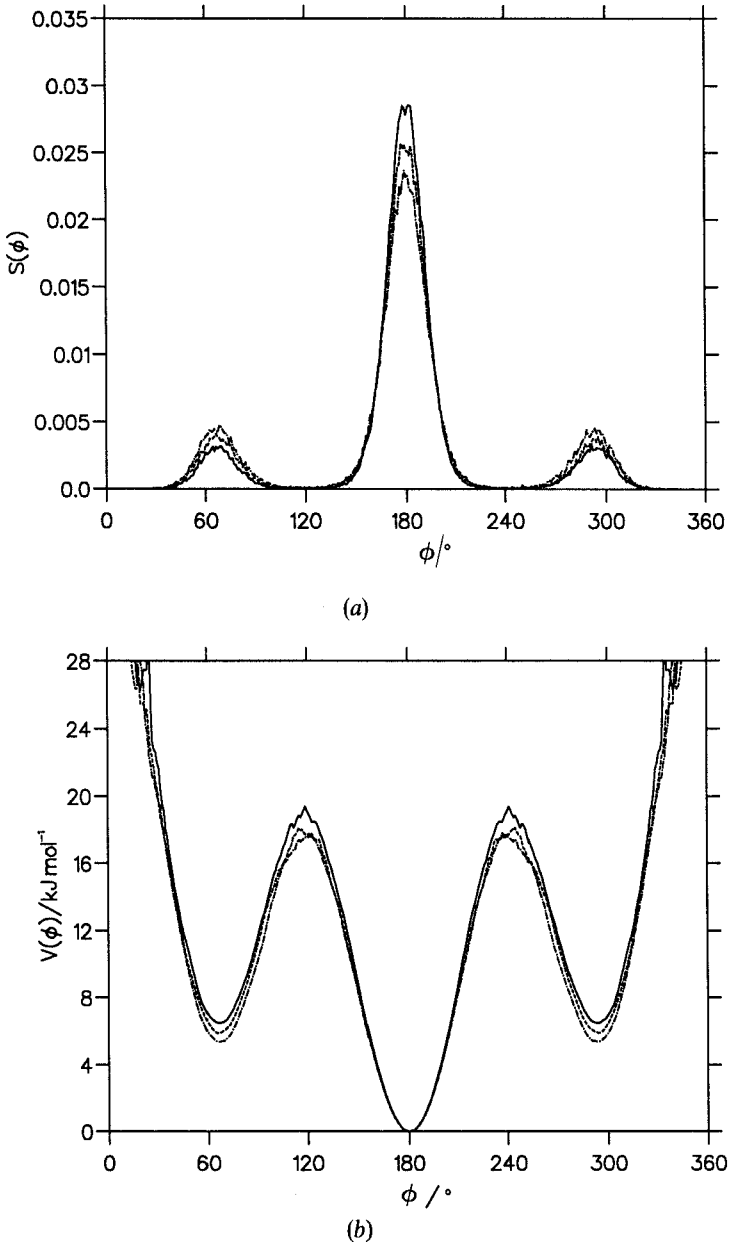

Figure 2. Torsional angle data for angle 16–17–18–19 at 350 K (full line), 370 K (dashed line), and 390 K (dot–dashed line). (*a*) Dihedral angle distribution $\mathscr{S}(\phi)$, (mole fraction per degree). (*b*) Effective torsional potential $\mathscr{V}(\phi)$ (smoothed and symmetrized).

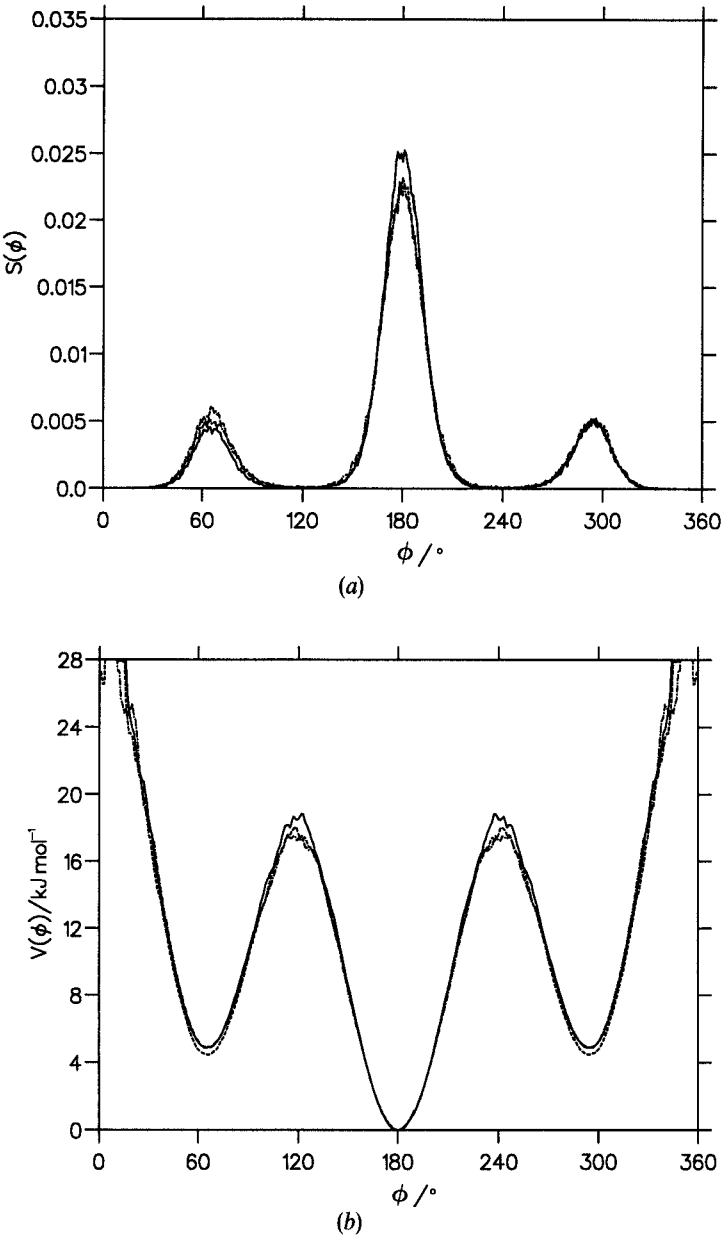

Figure 3. Torsional angle data for angle 15–16–17–18 at 350 K (full line), 370 K (dashed line), and 390 K (dot–dashed line). (*a*) Dihedral angle distribution $\mathscr{S}(\phi)$, (mole fraction per degree). (*b*) Effective torsional potential $\mathscr{V}(\phi)$ (smoothed and symmetrized).

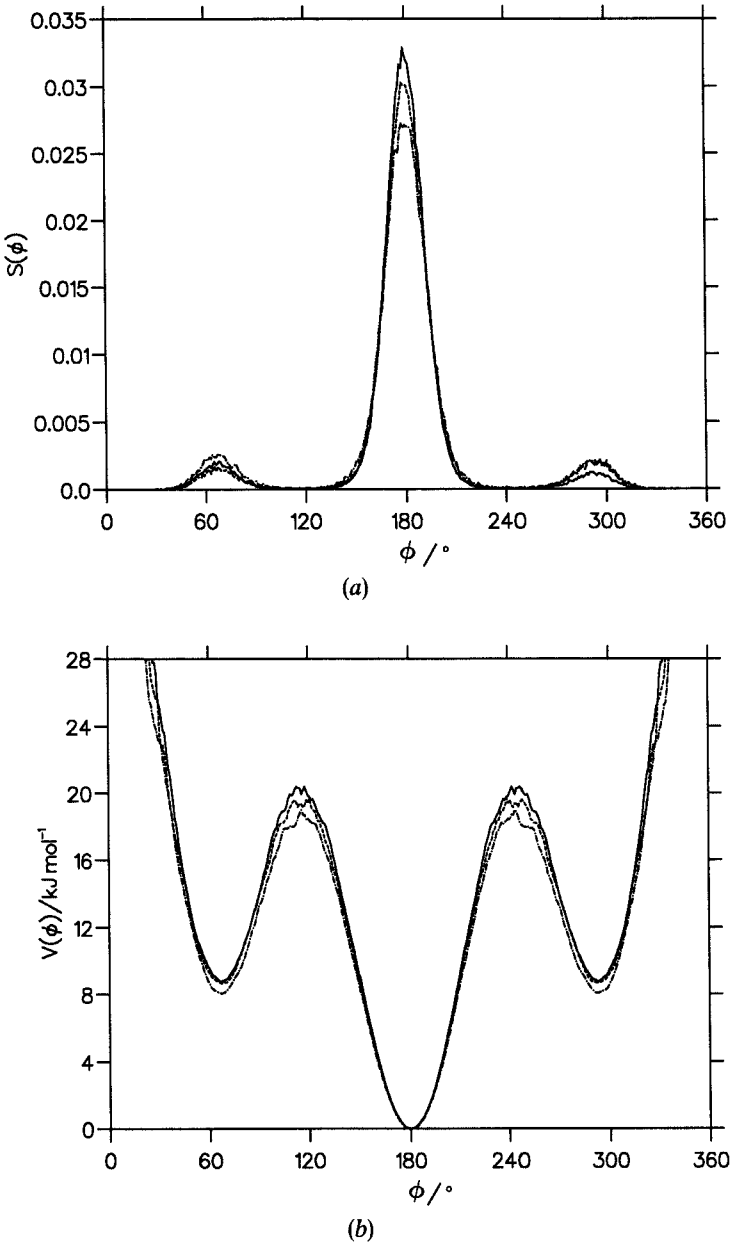

Figure 4. Torsional angle data for angle 12–15–16–17 at 350 K (full line), 370 K (dashed line), and 390 K (dot–dashed line). (*a*) Dihedral angle distribution $\mathscr{S}(\phi)$, (mole fraction per degree). (*b*) Effective torsional potential $\mathscr{V}(\phi)$ (smoothed and symmetrized).

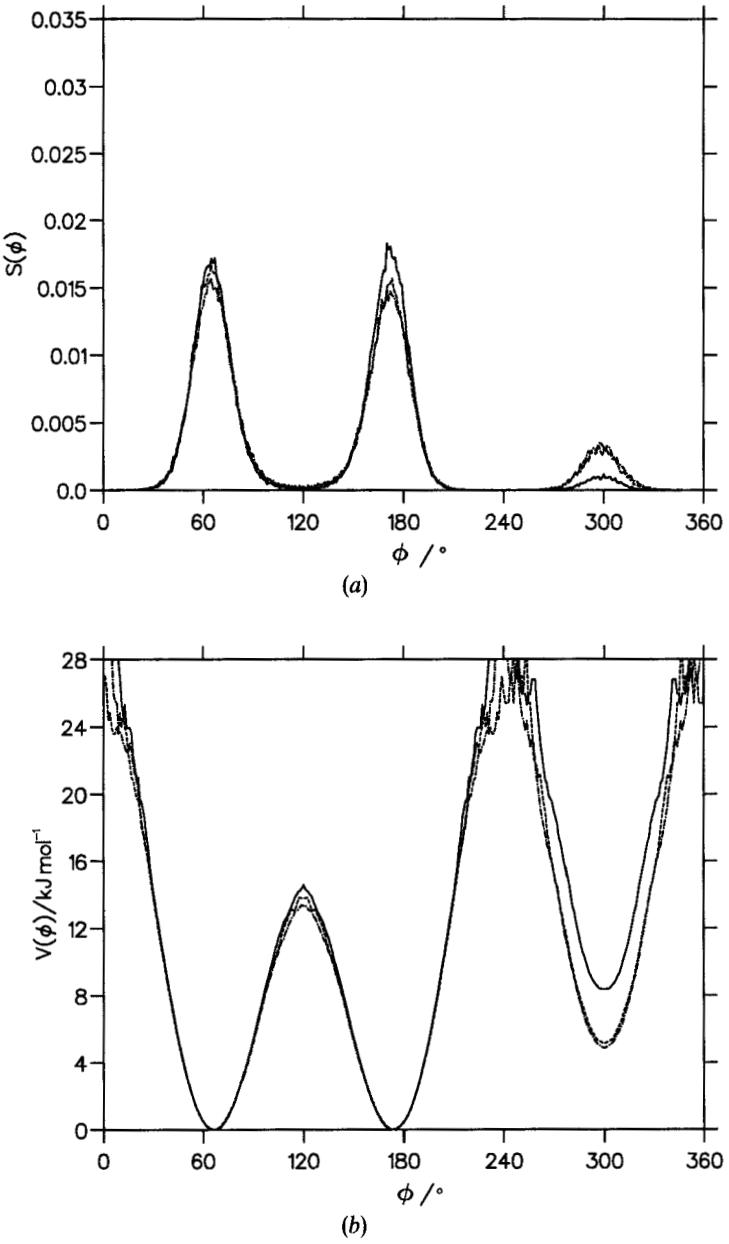

Figure 5. Torsional angle data for angle 11–12–15–16 at 350 K (full line), 370 K (dashed line), and 390 K (dot–dashed line). (*a*) Dihedral angle distribution $\mathscr{S}(\phi)$, (mole fraction per degree). (*b*) Effective torsional potential $\mathscr{V}(\phi)$ (smoothed and symmetrized).

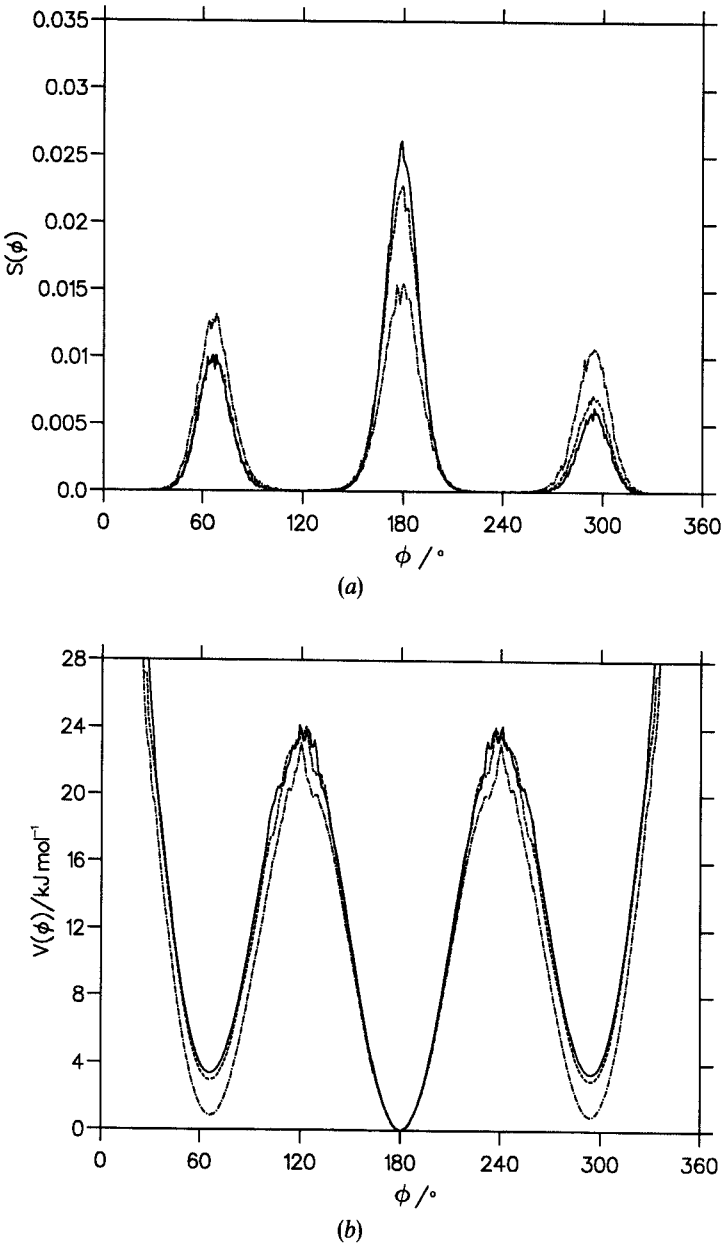

Figure 6. Torsional angle data for angle 5–6–9–14 at 350 K (full line), 370 K (dashed line), and 390 K (dot–dashed line). (*a*) Dihedral angle distribution $\mathscr{S}(\phi)$, (mole fraction per degree). (*b*) Effective torsional potential $\mathscr{V}(\phi)$ (smoothed and symmetrized).

173°. These findings correlate with both the crystal structure of CCH5 [15] and molecular mechanics calculations which we have carried out for different conformations of CCH5 using MM2 [16], which employs a much more sophisticated potential than can be used in the simulations. This confirms that our force field adequately models the intramolecular potential.

In general dihedral angle distributions become more smeared as the temperature is raised: higher molecular energies lead to the sampling of more *gauche* conformations. Integrating over the separate peaks of $\mathscr{P}(\phi)$ allows the calculation of the percentage of *gauche* and *trans* conformations for each angle; these are given in table 1. Relative statistical weights of different conformations are obtained by periodic sampling during the course of a molecular dynamics run. These are tabulated in table 2 (chain conformations only) and in table 3 (all conformations). As expected, the alkyl chain strongly prefers an all-*trans* conformation. In the nematic phase at 350 K almost 50 per cent of molecules are found to have a fully extended alkyl chain. These figures are significantly higher than those predicted by Emsley *et al.* [17] for 5CB based on the rotameric state model introduced by Flory, but are similar to values obtained for *n*-pentane at 25°C [18].

The ordering of *gauche* angle populations is somewhat surprising. One might intuitively expect that the end torsional angle 16–17–18–19 would be the most disordered of the chain dihedrals; indeed such an effect appears to be shown for *n*-hexane [18]. However, in this work the angle 15–16–17–18 is the most disordered of the chain dihedrals, an effect best understood in terms of differences in effective torsional potentials $\mathscr{V}(\phi)$ described later. Again it is interesting to compare these results with those from the rotameric state model. The latter predicts equal weights for all single *gauche* conformations in the isotropic phase, but in the presence of a nematic mean field predicts the same ordering of chain dihedral angle populations as we obtain in this study.

The effective torsional potentials provide a probe of local structural changes in the environment of a molecule. Significant changes in $\mathscr{V}(\phi)$ as a function of temperature were seen in four of the angles considered. In figure 2(*b*), the effective torsional potential for the end of chain dihedral angle 16–17–18–19 changes shape as the temperature is lowered and the nematic phase is entered. The energy gap between *gauche* and *trans* conformations is increased and the energy barrier between interconversion of *gauche* and *trans* conformations is raised. This phenomenon can be directly assigned to the effect of the nematic molecular field, which causes alignment of molecules along the director. As the order parameter increases a quenching of *gauche* conformations occurs. It becomes energetically less favourable for *gauche* conformations to exist because the 18–19 bond must lie at an angle to the nematic molecular field. Similar quenching effects can be seen for angles 12–15–16–17, 11–12–15–16 and 5–6–9–14. In table 4 we attempt to quantify this by tabulating the free energy difference between energy minima $\Delta\mathscr{V}_{\min}$, for each angle. For four of the angles $\Delta\mathscr{V}_{\min}$ corresponds to the mean difference between *gauche* and *trans* energy minima, whereas for the angle 11–12–15–16 $\Delta\mathscr{V}_{\min}$ represents the difference between the energy minima at $\phi = 67°$, 173° and the energy minimum at 300°. For the angle 16–17–18–19 a steady increase in seen in $\Delta\mathscr{V}_{\min}$ in going from 390 K to 370 K to 350 K. However, for the angles 12–15–16–17 and 5–6–9–14 the major change in $\Delta\mathscr{V}_{\min}$ occurs between 390 K and 370 K. *Gauche* conformations for these two angles have a very large influence on the overall linearity of the molecule: we therefore expect the main quenching of these dihedral angles to occur when molecules start to align as the nematic phase is entered.

Table 1. *Trans* and *gauche* dihedral angle populations g^- and g^+ conformations are defined respectively for $\phi \leqslant 120°$ and $\phi \geqslant 240°$.

Angle	T/K	g^-/%	t/%	g^+/%
16–17–18–19	350	8·8	82·3	8·9
16–17–18–19	370	11·5	77·9	10·6
16–17–18–19	390	13·9	72·8	13·2
15–16–17–18	350	12·6	73·0	14·3
15–16–17–18	370	16·9	68·2	14·9
15–16–17–18	390	15·4	69·7	15·0
12–15–16–17	350	5·4	91·3	3·4
12–15–16–17	370	4·5	89·4	6·2
12–15–16–17	390	7·6	86·2	6·2
11–12–15–16	350	48·0	49·4	2·6
11–12–15–16	370	48·2	43·8	8·0
11–12–15–16	390	46·5	44·2	9·3
5–6–9–14	350	23·3	63·2	13·5
5–6–9–14	370	24·3	58·8	16·9
5–6–9–14	390	31·7	41·9	26·4

Table 2. Relative populations of chain conformations.

Angle 12–15–16–17	Angle 15–16–17–18	Angle 16–17–18–19	% at 350 K	% at 370 K	% at 390 K
g^-	g^-	g^-	0·2	0·0	0·2
g^-	g^-	t	1·2	0·9	0·8
g^-	g^-	g^+	0·2	0·0	0·0
g^-	t	g^-	0·4	0·3	1·0
g^-	t	t	2·9	2·5	4·4
g^-	t	g^+	1·1	0·7	1·1
g^-	g^+	g^-	0·0	0·0	0·0
g^-	g^+	t	0·0	0·1	0·1
g^-	g^+	g^+	0·0	0·0	0·0
t	g^-	g^-	1·6	2·2	2·9
t	g^-	t	14·2	13·7	11·3
t	g^-	g^+	0·6	0·1	0·1
t	t	g^-	6·2	8·1	8·9
t	t	t	49·2	44·4	41·3
t	t	g^+	5·3	7·3	8·3
t	g^+	g^-	0·0	0·1	0·1
t	g^+	t	11·3	11·6	10·7
t	g^+	g^+	1·5	1·8	2·6
g^+	g^-	g^-	0·1	0·0	0·0
g^+	g^-	t	0·6	0·0	0·1
g^+	g^-	g^+	0·1	0·0	0·0
g^+	t	g^-	0·7	0·8	0·8
g^+	t	t	1·8	3·4	2·9
g^+	t	g^+	0·3	0·6	0·9
g^+	g^+	g^-	0·0	0·0	0·0
g^+	g^+	t	0·4	1·3	1·4
g^+	g^+	g^+	0·0	0·0	0·2

Table 3. Relative populations of most popular conformations for the five key dihedral angles. Only conformations with populations of 1 per cent or more at (at least) one temperature are included.

Angle 5–6–9–14	Angle 11–12–15–16	Angle 12–15–16–17	Angle 15–16–17–18	Angle 16–17–18–19	% at 350 K	% at 370 K	% at 390 K
g^-	g^-	g^-	t	t	0·4	0·6	1·3
g^-	g^-	t	g^-	t	1·1	2·2	1·8
g^-	g^-	t	t	g^-	0·7	0·9	1·3
g^-	g^-	t	t	t	6·2	5·4	6·3
g^-	g^-	t	g^+	t	1·2	1·6	1·4
g^-	t	t	g^-	t	2·8	1·4	1·9
g^-	t	t	t	g^-	0·7	0·7	1·4
g^-	t	t	t	t	5·7	4·5	7·0
g^-	t	t	g^+	t	1·0	1·0	1·0
t	g^-	g^-	t	t	2·1	1·6	1·6
t	g^-	t	g^-	t	3·5	3·3	1·9
t	g^-	t	t	g^-	2·2	3·3	2·0
t	g^-	t	t	t	13·8	13·1	8·1
t	g^-	t	t	g^+	1·3	2·4	2·2
t	g^-	t	g^+	t	3·4	3·4	2·5
t	t	t	g^-	t	5·1	4·0	1·8
t	t	t	t	g^-	1·5	2·1	1·5
t	t	t	t	t	15·2	9·2	7·3
t	t	t	t	g^+	2·4	1·9	1·3
t	t	t	g^+	t	3·7	2·5	2·3
t	t	g^+	t	t	1·4	2·4	1·0
t	g^+	t	t	t	0·7	1·7	1·9
g^+	g^-	g^-	t	t	0·4	0·2	1·2
g^+	g^-	t	g^-	t	0·2	0·3	1·3
g^+	g^-	t	t	g^-	0·3	0·2	1·0
g^+	g^-	t	t	t	3·1	3·9	3·6
g^+	t	t	g^-	t	1·0	1·1	1·5
g^+	t	t	t	t	4·1	4·4	4·8
g^+	t	t	t	g^+	0·3	0·2	1·3
g^+	t	t	g^+	t	0·9	1·4	1·5
g^+	g^+	t	t	t	0·1	1·3	1·3

The most dramatic change in $\mathscr{V}(\phi)$ occurs for the angle 11–12–15–16 between 370 K and 350 K, where $\Delta\mathscr{V}_{min}$ increases by over 3 kJ mol^{-1}. In the high energy, symmetrical, g^+ conformation of this angle the alkyl chain (if all-*trans*) projects away from the axis defined by the rigid core. Packing effects make this conformation unlikely, and it becomes especially so in the ordered nematic phase.

The relative values of $\Delta\mathscr{V}_{min}$ for chain dihedrals are instructive. $\mathscr{V}(\phi)$ is lowest for the angle 15–16–17–18. In this work the same third order Fourier term was used in equation (1) for all angles; differences in $\mathscr{V}(\phi)$ must therefore be assigned to a combination of intra- and intermolecular non-bonded interactions. In an attempt to separate intra- from intermolecular effects, we extracted individual molecular conformations from our dynamics data and used these conformations as starting points for energy minimization calculations using the molecular mechanics module of the program AMBER. In table 5 we give the dihedral angles and relative energies for four energy minima. A difference in energy between *gauche* conformations is discernible, though this is relatively small. In the gas phase, long range chain/core non-bonded

Table 4. Angles of the absolute energy minima ϕ_{min}, of the metastable energy minima ϕ'_{min}, and the energy differences $\Delta\mathscr{V}_{min}$, for different torsional angles at 350 K, 370 K and 390 K.

Angle	T/K	ϕ_{min}/°	ϕ'_{min}/°	$\Delta\mathscr{V}_{min}$/kJ mol^{-1}
16–17–18–19	350	180	66, 294	6·48
16–17–18–19	370	180	66, 294	5·90
16–17–18–19	390	180	66, 294	5·38
15–16–17–18	350	180	66, 294	4·89
15–16–17–18	370	180	66, 294	4·46
15–16–17–18	390	180	65, 295	4·86
12–15–16–17	350	180	67, 293	8·77
12–15–16–17	370	180	67, 293	8·65
12–15–16–17	390	180	67, 293	8·05
11–12–15–16	350	67, 173	300	8·37
11–12–15–16	370	67, 173	300	5·13
11–12–15–16	390	67, 173	300	4·85
5–6–9–14	350	180	66, 294	3·40
5–6–9–14	370	180	66, 294	2·98
5–6–9–14	390	180	66, 294	0·83

Table 5. Relative energies $\Delta\mathscr{V}$ for energy minimised conformations of CCH5 in the gas phase.

	ϕ/°					
	5–6–9–14	11–12–15–16	12–15–16–17	15–16–17–18	16–17–18–19	$\Delta\mathscr{V}$/kJ mol^{-1}
ttttt	179·0	172·9	179·8	180·1	180·0	0·00
ttttg^-	179·1	173·0	179·6	180·4	65·3	2·91
tttg^-t	179·1	172·8	180·1	64·6	180·2	2·42
ttg^+tt	179·1	171·7	295·6	179·4	180·2	1·31

interactions serve to stabilise *gauche* bonds closest to the core; however in CCH5 it would appear that molecular packing effects in the nematic phase are much more significant. In CCH5 the balance of these energetic effects favour the *gauche* conformations for the middle dihedral angle 15–16–17–18. For this angle introduction of a *gauche* conformation does not cause a significant deviation from linearity for the molecule and we are therefore unable to detect a noticeable nematic field effect on $\Delta\mathscr{V}_{min}$.

It is also possible to estimate the height of the conformational energy barrier $\Delta\mathscr{V}_{barrier}$ from the graphs in figures 2(*b*)–6(*b*). These quantities are subject to greater statistical uncertainty than $\Delta\mathscr{V}_{min}$ because sampling of dihedral angles is necessarily poorer. Despite this it seems clear than for each angle the barrier to rotation is raised at 350 K, where the nematic phase is entered. In this work we do not attempt to plot the height of the barrier between *gauche* conformations at 0° or the height of the barrier at 240° for angle 11–12–15–16, where sampling is particularly poor. However, we would also expect a similar increase in energy for these barriers.

3. The equivalent inertia spheroid

It is possible to obtain an approximate measure of overall molecular shape by using the second moments of the atomic mass distribution (about the centre of mass) to construct an equivalent spheroid. The spheroid is defined to have a uniform mass

density, the same total mass, and the same moments of inertia, as the molecule. The lengths of the principal axes of the spheroid give estimates of the molecular 'length', 'width' and 'breadth'.

The precise prescription is as follows. For each molecule, the inertia tensor I is defined

$$I_{\alpha\beta}=\sum_i m_i(r_i^2\delta_{\alpha\beta}-r_{i\alpha}r_{i\beta}). \tag{3}$$

The sum is over all atoms i in the molecule, $\alpha,\beta=x,y,z$, and the positions $\mathbf{r}_i$ are measured relative to the centre of mass. For our potential model, hydrogen atoms are not explicitly included: they are absorbed into CH, CH_2 and CH_3 groups. Accordingly we sum over these 19 united atoms. For simplicity we take all of the masses m_i to be equal. This choice is arbitrary, and it is worth recalling that properly defined static classical ensemble averages are independent of the mass distribution. Here we ascribe no physical meaning to the mass, but simply use it to give a reasonable statistical weighting to each atom. (In the molecular dynamics simulations the proper united atom masses were used.)

Having constructed the inertia tensor for each molecule, it is diagonalized. This procedure yields three eigenvectors **a**, **b** and **c**, the principal molecular axis vectors; the three corresponding eigenvalues are the respective principal moments of inertia I_{aa}, I_{bb} and I_{cc}. A solid body, in the shape of a spheroid with semi-axes of length, a, b and c, and total mass

$$M=\sum_i m_i,$$

has moments of inertia given by $I_{aa}/M=(b^2+c^2)/5$ and cyclic permutations. Accord-changes take place. Accordingly, the distinction between b and c axes is a conform-inertia for each molecule: $a=\sqrt{[2{\cdot}5(I_{bb}+I_{cc}-I_{aa})/M]}$ and cyclic permutations thereof. The molecule length, width and breadth are respectively $2a$, $2b$ and $2c$. These quantities were reported in our original paper [11] and for convenience we tabulate them again in table 6 at the three temperatures under study. We note that the molecule becomes longer and narrower as the temperature is reduced, and as the system goes from the isotropic to the nematic phase. This is consistent with the torsional angle distributions described in the previous section.

Here, we investigate further the nature of the change in shape, by focusing attention on the distribution of molecular width and breadth, b and c. This is measured by accumulating two dimensional histograms and converting to a normalized probability distribution $f(b,c)$. Two dimensional contour plots of $f(b,c)$ are shown in figure 7 for the temperatures 390 K (isotropic phase) and 350 K (nematic phase), together with a difference density map $f_{350}-f_{390}$ for these two temperatures. First, we note that the highest probability density (region 1 in the figure) occurs for unsymmetrical shapes,

Table 6. Length, width and breadth of equivalent inertia spheroid.

T/K	$2a$/Å	$2b$/Å	$2c$/Å
350	19·60	4·12	2·24
370	19·46	4·18	2·36
390	19·32	4·22	2·54

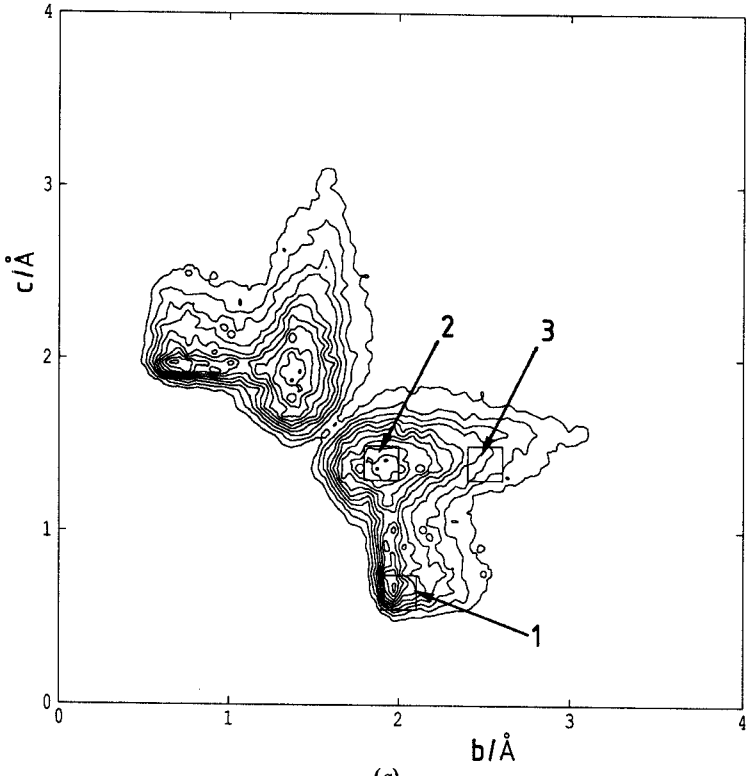

(*a*)

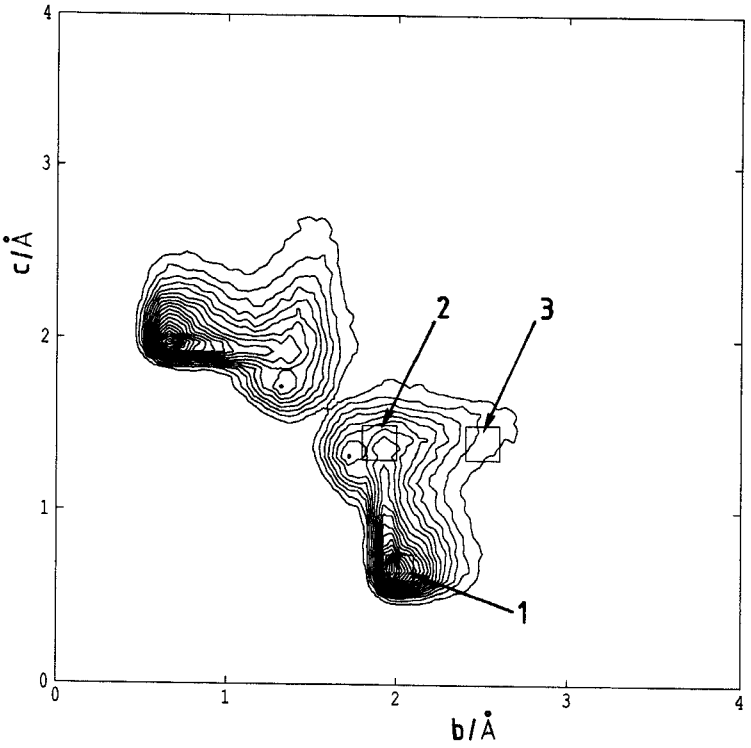

(*b*)

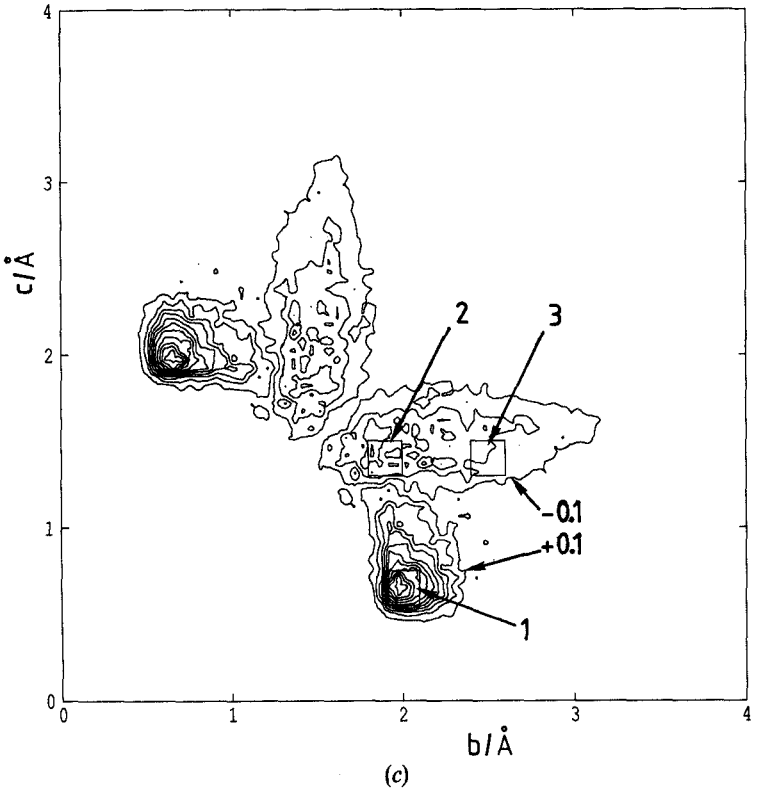

(*c*)

Figure 7. Contour plots of the normalized probability density $f(b, c)$ for the molecular shape as measured by the equivalent inertia spheroid b and c axes. (*a*) $T = 390$ K, isotropic phase, with contours at $f = 0{\cdot}2, 0{\cdot}4, 0{\cdot}6 \ldots$. (*b*) $T = 350$ K, nematic phase, with contours at $f = 0{\cdot}2, 0{\cdot}4, 0{\cdot}6 \ldots$. (*c*) Difference density between (*a*) and (*b*), with contours at $f = \pm 0{\cdot}1$ (marked), $\pm 0{\cdot}3, \pm 0{\cdot}5 \ldots$. In each case regions 1 (peak), 2 (ridge) and 3 (ridge) as indicated.

$b \neq c$, but that the contours extend to the symmetry line $b = c$, so smooth interconversions of molecular width and breadth occur from time to time, as conformational changes take place. Accordingly, the distinction between b and c axes is a conformational, rather than configurational, one. Secondly, we note the presence of a ridge of probability density, extending from region 2 to region 3 in the figure, corresponding to molecules somewhat broader than the average. A major difference between the distributions at the two different temperatures is the transfer of probability density between this ridge and the high probability peak. Torsional angle distribution have been calculated for molecules in specific regions of this map (see figure 7 and table 7). Unsurprisingly, the most probable conformations, represented by region 1, have all the dihedral angles close to their lowest energy values. An exception is the 15–16–17–18 angle, which has some freedom as discussed in the previous section. The ridge consists of molecules with a higher proportion of *gauche* conformers, especially for the 6–9 bond between the cyclohexane rings, with different positions along the ridge corresponding to different combinations of alkyl tail conformers. In region 2 the chain-end torsion 16–17–18–19 is activated a little compared with the peak; in region 3 both this and the 12–15–16–17 bond are more twisted. These degrees of freedom are quenched in the nematic phase, so the ridge becomes shorter.

Table 7. *Trans/gauche* dihedral angle populations in specific regions of (b, c) space.

Region 1 (peak): $b=2{\cdot}0\pm0{\cdot}1$, $c=0{\cdot}65\pm0{\cdot}1$			
Angle	g^-/%	g^+/%	t/%
5–6–9–14	0	0	100
11–12–15–16	50	0	50
12–15–16–17	0	0	100
15–16–17–18	15	15	70
16–17–18–19	0	0	100
Region 2 (ridge): $b=1{\cdot}9\pm0{\cdot}1$, $c=1{\cdot}4\pm0{\cdot}1$			
Angle	g^-/%	g^+/%	t/%
5–6–9–14	50	30	20
11–12–15–16	45	10	45
12–15–16–17	0	0	100
15–16–17–18	15	15	70
16–17–18–19	10	10	80
Region 3 (ridge): $b=2{\cdot}5\pm0{\cdot}1$, $c=1{\cdot}4\pm0{\cdot}1$			
Angle	g^-/%	g^+/%	t/%
5–6–9–14	40	40	20
11–12–15–16	50	10	40
12–15–16–17	25	15	60
15–16–17–18	5	0	95
16–17–18–19	20	15	65

4. Bond orientational distributions

To describe the distribution of molecular orientations we must first determine the director. For rigid, axially symmetric molecules this is straightforwardly accomplished by diagonalizing the ordering tensor whose components are

$$Q^{aa}_{\alpha\beta}=\frac{1}{N}\sum_{j=1}^{N}\frac{3}{2}a_{j\alpha}a_{j\beta}-\frac{1}{2}\delta_{\alpha\beta}, \tag{4}$$

where N is the number of molecules and $\mathbf{a}_j$ the axial unit vector. For flexible molecules lacking a symmetry axis we must define a molecule based axis system. We use the inertia tensor of the previous section for this purpose, identifying $\mathbf{a}_j$, $\mathbf{b}_j$ and $\mathbf{c}_j$ as the principal molecular axes. This then leads to a generalization of equation (4) [19]

$$Q^{uv}_{\alpha\beta}=\frac{1}{N}\sum_{j=1}^{N}\frac{3}{2}u_{j\alpha}v_{j\beta}-\frac{1}{2}\delta_{\alpha\beta}\delta_{uv}, \tag{5}$$

where $\mathbf{u}_j, \mathbf{v}_j = \mathbf{a}_j, \mathbf{b}_j$ or $\mathbf{c}_j$. Hashim *et al.* [20], used this approach in their study of biaxial molecules on a lattice (for which the axes $\mathbf{a}_j$, $\mathbf{b}_j$ and $\mathbf{c}_j$ are defined *a priori*). In a laboratory frame having the director as its z axis, and neglecting the (small) biaxiality induced by finite system size, *each* of the 3×3 submatrices $\mathbf{Q}^{uv}$ is diagonal [19] with

$$Q^{uv}_{zz}=-2Q^{uv}_{xx}=-2Q^{uv}_{yy}.$$

Hence, to locate the director, we simply need to diagonalize one of these submatrices, and the most convenient choice is based on the long axes $\mathbf{a}_j$ of the molecules, which are clearly identifiable from the analysis of the inertia tensor. The director $\mathbf{n}$ is the eigenvector associated with the largest eigenvalue of $\mathbf{Q}^{aa}$, the tensor defined by equations (4) and (5) with $\mathbf{u}_j = \mathbf{v}_j = \mathbf{a}_j$. Order parameters and distributions are then referred to angles between molecular vectors and $\mathbf{n}$. At 350 K we found an overall molecular order parameter

$$S \equiv \langle P_2(\mathbf{n} \cdot \mathbf{a}) \rangle \equiv \langle Q_{zz}^{aa} \rangle = 0{\cdot}66$$

Other diagonal elements adopted the expected values

$$\langle Q_{xx}^{aa} \rangle \approx \langle Q_{yy}^{aa} \rangle \approx \langle Q_{zz}^{bb} \rangle \approx \langle Q_{zz}^{cc} \rangle \approx -\frac{1}{2} S = -0{\cdot}33$$

and

$$\langle Q_{xx}^{bb} \rangle \approx \langle Q_{yy}^{bb} \rangle \approx \langle Q_{xx}^{cc} \rangle \approx \langle Q_{yy}^{cc} \rangle \approx \frac{1}{4} S = 0{\cdot}17$$

with the off-diagonal elements essentially zero. For a non-rigid molecule a single order parameter is not sufficient [19]: one must calculate orientational distributions and average for a variety of vectors embedded in the molecular structure. We turn to this next.

We have calculated the molecular orientational distribution function $f(\cos\theta)$ where θ is the angle between $\mathbf{a}$ and the director, and in addition computed this function for each carbon–carbon bond along the alkyl chain, for the 12–19 vector stretching from end to end of the alkyl chain, for the 6–9 bond joining the two cyclohexane rings, and for the 1–2 vector (the polar CN group). The results for 350 K are shown in figure 8. In addition, orientational order parameters $\langle P_2(\cos\theta) \rangle$ and $\langle P_4(\cos\theta) \rangle$ (second and fourth rank Legendre polynomials) are given in table 8. It can be seen that the distributions for the $\mathbf{a}$ vector, for the overall alkyl tail 12–19 vector, for the 6–9 vector, and the 1–2 vector, are similar, and peaked around $\theta = 0$ as expected. The $\mathbf{a}$ vector distribution is the sharpest, consistent with the use of $\mathbf{a}$ to define the director. Alternate bonds (12–15, 16–17, 18–19) along the alkyl chain also have orientational distributions peaked along the director, although the distributions become groader (and the order parmaeters lower) the further one looks along the chain. The remaining bonds (15–16 and 17–18) are distributed about a tilted orientation: on average they stick out at an angle to the director. This is expected, and should be related to the odd–even effect in its various manifestations.

We have carried out least squares fits of the function $f(\cos\theta)$ to the form

$$f(\cos\theta) = c \exp\{a_2 P_2(\cos\theta) + a_4 P_4(\cos\theta) + \ldots\}, \tag{6}$$

where c is a normalization constant; the results for the coefficients a_i are included in table 8. The Maier–Saupe theory [1] assumes such a functional form with a_2 the only non-zero coefficient, determined by the value of $\langle P_2 \rangle$. However, as discussed by Eppenga and Frenkel [21], the same function would result from an information theory approach, while Sluckin and Shukla [22] have shown how it arises in density functional theory, so its significance is not related to the validity or otherwise of Maier–Saupe theory. We find that, for most of the vectors examined here, an excellent fit is obtained using just the terms given explicitly in equation (6). Higher order terms do not

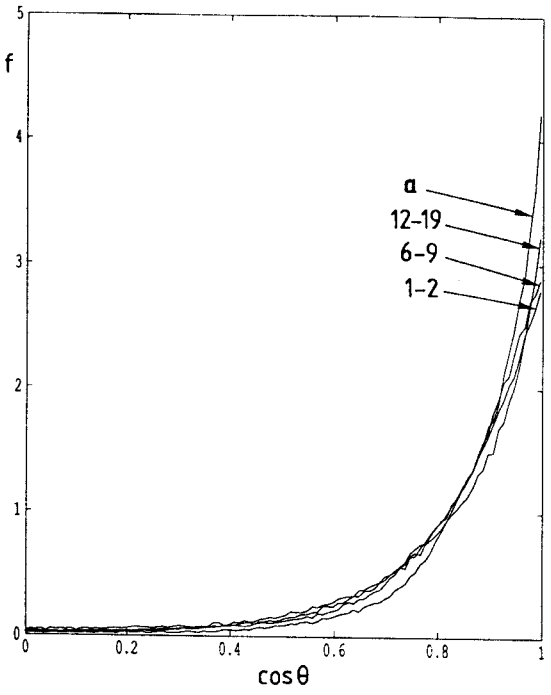

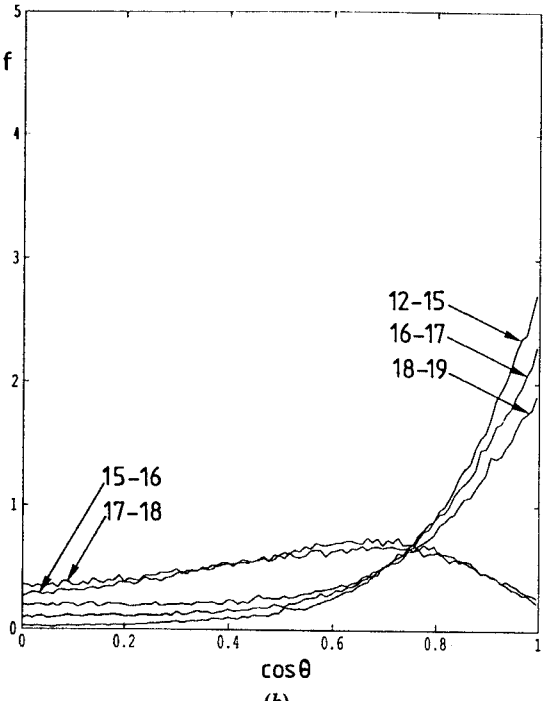

Figure 8. Orientational distribution functions $f(\cos\theta)$ at 350 K, for vectors defined in the molecular framework. (*a*) The equivalent inertia spheroid **a** axis, the 1–2, 6–9 bonds, and the 12–19 vector. (*b*) Successive bonds down the alkyl chain.

Table 8. Order parameters and $f(\cos\theta)$ fit coefficients at 350 K.

Vector	$\langle P_2(\cos\theta)\rangle$	$\langle P_4(\cos\theta)\rangle$	a_2	a_4	a_6
a vector	0·66	0·28	3·74	−0·244	
1–2 bond	0·57	0·18	3·37	−0·474	
6–9 bond	0·60	0·20	3·18	−0·465	
12–19 vector	0·55	0·19	2·84	−0·273	
12–15 bond	0·57	0·17	3·27	−0·607	0·135
15–16 bond	0·35	−0·10	0·17	−0·949	
16–17 bond	0·48	0·14	2·23	−0·040	−0·249
17–18 bond	0·21	−0·07	0·09	−0·710	
18–19 bond	0·38	0·11	1·60	−0·267	−0·235

significantly improve the fit, so a knowledge of $\langle P_2\rangle$ and $\langle P_4\rangle$ is sufficient to determine the full form of $f(\cos\theta)$. This applies to all the functions displayed in figure 8 (*a*); moreover $|a_4| \ll |a_2|$ in all these cases. The 15–16 and 17–18 distributions in figure 8 (*b*) which have quite a different shape, also do not require higher order terms, but here $|a_4\rangle \gg |a_2|$. The remaining three distributions, for the 12–15, 16–17 and 18–19 bonds, require a term in $a_6P_6(\cos\theta)$ for a satisfactory fit.

5. Conclusions

We have carried out molecular dynamics simulations for the mesogen CCH5 in both the nematic and isotropic phases using realistic atom–atom potentials which model both intermolecular and intramolecular interactions. A wealth of structural data is available from these simulations. We observe differences in both dihedral angle distributions and the equivalent moment of inertia spheroid for CCH5 at different temperatures. These differences are partly due to simple temperature effects and partly due to changes in the effective torsional potentials experienced by CCH5 molecules. The latter can be traced to the change in the molecular environment of CCH5 molecules as the nematic phase is entered. In going from the isotropic to the nematic phase there is a quenching of those *gauche* conformations which cause part of the chain to lie at an angle to the nematic molecular field. CCH5 is therefore seen to undergo a change in shape and become more elongated in the nematic phase.

Calculated bond orientational distributions for the alkyl chain show a pronounced odd–even effect. Addition of extra atoms to the chain would add bonds alternately parallel to, and at an angle to, the director, causing an uneven increase in molecular length. This effect would become smaller as the alkyl chain becomes longer and bond orientational distributions become more diffuse. We find that, even for the short C_5 chain in CCH5, *gauche* conformations can be stabilized through interactions with the core of the molecule and destabilized by molecular packing constraints. With longer chains the extra dihedral angles are likely to make these effects even more important. In some systems packing constraints and chain/core interactions may be more important in determining molecular length and molecular polarizability anisotropy than the odd–even effect itself; this may therefore explain the breakdown of the odd–even effect in transition temperatures of certain homologous series. Further simulations of realistic atom–atom models may help to unravel such phenomena.

The authors would like to thank the University of Bristol Computing Service for the provision of computer time and the support of this project. M.R.W. would like to thank

the U.K. S.E.R.C. for financial assistance through the award of a Research Fellowship (1988–90), and Lancaster University for travel grants.

References

[1] MAIER, W., and SAUPE, A., 1958, *Z. Naturf.* (*a*), **13**, 564; 1959, *Ibid.*, **14**, 882; 1960, *Ibid.*, **15**, 287.
[2] DE GENNES, P. G., 1971, *Molec. Crystals liq. Crystals*, **12**, 193.
[3] SHENG, P., and PRIESTLEY, E. B., 1979, *Introduction to Liquid Crystals*, edited by E. B. Priestley, P. J. Wojtowitz and P. Sheng (Plenum Press), Chap. 10.
[4] ONSAGER, L., 1949, *Ann. N.Y. Acad. Sci.*, **51**, 627.
[5] For a review see: ALLEN, M. P., and WILSON, M. R., 1989, *J. Comput. Aided Molec. Design*, **3**, 335.
[6] LEBWOHL, P. A., and LASHER, G., 1972, *Phys. Rev.* A, **6**, 426; 1973, *Ibid.*, **7**, 2222. LUCKHURST, G. R., and SIMPSON, P., 1982, *Molec. Phys.*, **47**, 251. FABBRI, U., and ZANNONI, C., 1986, *Molec. Phys.*, **58**, 763.
[7] FRENKEL, D., MULDER, B. M., and MCTAGUE, J. P., 1984, *Phys. Rev. Lett.*, **52**, 287. FRENKEL, D., and MULDER, B. M., 1985, *Molec. Phys.*, **55**, 1171.
[8] FRENKEL, D., 1987, *Molec. Phys.*, **60**, 1. STROOBANTS, A., LEKKERKERKER, H. N. W., and FRENKEL, D., 1987, *Phys. Rev.* A, **36**, 2929. FRENKEL, D., LEKKERKERKER, H. N. W., and STROOBANTS, A., 1988, *Nature, Lond.*, **332**, 822. FRENKEL, D., 1988, *J. Phys. Chem.*, **92**, 3280.
[9] ALLEN, M. P., and FRENKEL, D., 1988, *Phys. Rev.* A, **37**, 1813; 1990, *Ibid.*, **42**, 3641E. ALLEN, M. P., FRENKEL, D., and TALBOT, J., 1989, *Comput. Phys. Rep.*, **9**, 301. ALLEN, M. P., 1990, *Liq. Crystals*, **8**, 499. ALLEN, M. P., 1990, *Phys. Rev. Lett.*, **65**, 2881.
[10] WILSON, M. R., and DUNMUR, D. A., 1989, *Liq. Crystals*, **5**, 987. DUNMUR, D. A., and WILSON, M. R., 1989, *Molec. Simul.*, **4**, 37.
[11] WILSON, M. R., and ALLEN, M. P., 1991, *Molec. Crystals liq. Crystals*, **198**, 465 (*Proceedings of the 13th International Liquid Crystal Conference*).
[12] SINGH, U. C., WEINER, P. K., CALDWELL, J., and KOLLMAN, P. A., 1987, *AMBER 3.0*, University of California–San Francisco.
[13] RYCKAERT, J. P., CICCOTTI, G., and BERENDSEN, H. J. C., 1977, *J. comput. Phys.*, **23**, 327.
[14] ALLEN, M. P., and WILSON, M. R. (in preparation).
[15] HAASE, W., and PAULUS, H., 1983, *Molec. Crystals liq. Crystals*, **100**, 111.
[16] QCPE 423. MM2: *Molecular Mechanics* II (CDC Version of QCPE 395), modified by S. Profeta from the original program by N. L. Allinger and Y. H. Yub.
[17] EMSLEY, J. W., LUCKHURST, G. R., and STOCKLEY, C. P., 1982, *Proc. R. Soc. Lond.* A, **381**, 117.
[18] JORGENSEN, W. L., MADURA, J. D., and SWENSON, C. J., 1984, *J. Am. chem. Soc.*, **106**, 6638.
[19] DE GENNES, P. G., 1974, *The Physics of Liquid Crystals* (Clarendon Press).
[20] HASHIM, R., LUCKHURST, G. R., and ROMANO, S., 1985, *Molec. Phys.*, **56**, 1217.
[21] EPPENGA, R., and FRENKEL, D., 1984, *Molec. Phys.*, **52**, 1303.
[22] SLUCKIN, T. J., and SHUKLA, P., 1983, *J. Phys.* A, **16**, 1539.